Enhanced machinability of SiC-reinforced metal-matrix composite with hybrid turning

Journal of Materials Processing Tech. 268 (2019) 149–161

Contents lists available at ScienceDirect

Journal of Materials Processing Tech.

journal homepage: www.elsevier.com/locate/jmatprotec

Enhanced machinability of SiC-reinforced metal-matrix composite with hybrid turning

Wei Bai[a,b], Anish Roy[b,*], Ronglei Sun[a], Vadim V. Silberschmidt[b]

[a] The State Key Lab of Digital Manufacturing Equipment and Technology, School of Mechanical Science and Engineering, Huazhong University of Science and Technology, Wuhan, 430074, China

[b] Wolfson School of Mechanical, Electrical and Manufacturing Engineering, Loughborough University, Leicestershire, LE11 3TU, UK

ARTICLE INFO

Associate Editor: Volker Schulze

Keywords:
Machinability
Particle-reinforced metal-matrix composites
Chip formation
Surface topography
Tool wear
Hybrid machining

ABSTRACT

Particle-reinforced metal-matrix composites are promising engineering materials thanks to their superior mechanical and thermal properties. However, their poor machinability is a deterrent for use in wider applications, due to the presence of hard ceramic particles, which results in rapid tool wear during machining. Ultrasonically assisted turning (UAT) is a hybrid machining technique, in which the cutting tool is made to vibrate at high frequencies and low amplitudes. In this study, the machinability and tool wear of machining SiCp/Al metal matrix-composite was compared for dry UAT and conventional turning with the use of a cemented carbide (WC) and a polycrystalline diamond (PCD) tool. With the use of ultrasonic assistance, a significant reduction in cutting forces was achieved with a slight increase in cutting temperature. Continuous and semi-continuous chips were obtained in UAT, with better surface topography. A chip-formation mechanism in UAT show increased ductility of the workpiece material when subjected to a repeated high-frequency microchipping process. Abrasive and adhesive wear occurred on the WC tool in both conventional turning and UAT. However, the machined surface obtained in UAT with a WC tool was comparable and sometimes even better than that achieved with the PCD tool.

1. Introduction

Metal-matrix composites (MMCs) are increasingly being used in various engineering applications, such as in aerospace, electronics and automotive industries thanks to their high specific strength, high stiffness, low thermal expansion, excellent corrosion and wear resistance. Chawla and Shen (2001) claim that particle-reinforced MMCs are often preferred to continuous-fibre-reinforced MMCs, because of their competitive advantage of low cost, ease of manufacture and nominal isotropic properties. Silicon carbide (SiC) particle-reinforced aluminium-matrix composites (SiCp/Al) have become a promising engineering material thanks to their outstanding mechanical properties and cost-effectiveness. Ozben et al. (2008) compared the varying reinforcement ratios of SiC particles on mechanical properties, concluding that an increase of reinforced volume fraction leads to improved mechanical properties such as impact toughness and hardness. However, Basavarajappa et al. (2006) pointed out that the presence of hard ceramic particles makes this material difficult to machine due to accelerated tool wear thereby limiting its widespread use in engineering applications.

Prior studies show that both extrinsic (cutting speed, feed rate, depth of cut and type of cutting tools) and intrinsic (particulate size, volume fraction and type of reinforcement) parameters influence machinability of particle reinforced MMCs. Manna and Bhattacharayya (2003) studied the influence of machining parameters, e.g. cutting speed, feed rate and depth of cut on the cutting force and surface finish criteria. They conclude that the use of rhombic tools have advantages in machining when cutting speeds range between 60 m/min to 150 m/min. Dabade and Joshi (2009) studied the effect of machining parameters and composite composition on chip formation and the effect of chip formation on surface roughness. They conclude that in machining of MMCs with coarser reinforcement lead to gross fracture with smaller chip segments and higher shear plane angle. El-Gallab and Sklad (1998) observed the cross-sections of the chips and found localization of the matrix deformation along shear bands, where the reinforcing SiC particles aligned themselves. Lin et al. (2001) observed that increasing a SiC volume fraction in the MMC lead to increased tool flank wear yielding increased surface roughness of the machined material. In all these studies, tool wear was deemed to be the primary drawback in machining MMCs, due to a highly abrasive nature of hard particulate

* Corresponding author.
E-mail address: a.roy3@lboro.ac.uk (A. Roy).

https://doi.org/10.1016/j.jmatprotec.2019.01.017
Received 20 August 2018; Received in revised form 26 December 2018; Accepted 26 January 2019
Available online 28 January 2019

reinforcements. Hocheng (2011) found polycrystalline diamond (PCD) and cubic boron nitride (CBN) tools perform much better than cemented carbide (WC) tools. Bhushan et al. (2010) reported that the flank wear of WC tool increased by a higher factor with the increase of cutting speed than that of PCD tool. However, due to the high cost of PCD tools, other tools such as cemented carbides and ceramics were also utilized to machine MMCs. Generally, there is a clear and tangible demand for cheaper and efficient machining of MMCs.

Hybrid machining, where a secondary process 'assists' a primary machining process has been a field of active research over the past decades. Ultrasonically assisted turning (UAT) is one such hybrid machining process, which demonstrated much promise in the machining of difficult-to-machine materials. Babitsky et al. (2003) describe a UAT setup which was shown to enhance the machinability of intractable material such as nickel superalloys. Thanks to the periodic separation of the tool and the workpiece at ultrasonic frequencies, the thermo-mechanical behaviour of the material in UAT differed significantly when compared with that in conventional turning (CT). Prior studies reported significant improvements of machining performances in UAT, such as cutting forces, surface finish and tool life. Maurotto et al. (2013) obtained over 70% of force reduction in UAT when compared to CT in the machining of Ti-alloys. In this regard, relatively few studies of UAT of MMCs are available. Zhao et al. (2002) studied the vibration-cutting performance of SiCp/Al; they concluded that ultrasonic cutting could reduce the influence of tearing, plastic deformation and built-up edge (BUE) and restrain chatter in the cutting process. Zhong and Lin (2006) observed that the surface roughness of an MMC sample obtained with UAT was better than that in CT.

The objective of this study is to compare and contrast the machinability of SiCp/Al MMC in CT and UAT with two different cutting tools types, with the aim of selecting a suitable tool by considering performance and cost-efficiency. To achieve this, a series of turning experiments under different machining conditions was studied. The machinability parameters, including cutting forces and temperatures, chip formation, surface roughness and topography, and tool wear for the two techniques were compared to reveal the advantages in machining with ultrasonic vibration.

2. Experimental setup and methodology

Machinability studies in turning of SiCp/Al were performed on a lathe appropriately modified to house an ultrasonic cutting head (Fig. 1). A schematic of the ultrasonically-assisted machining setup is illustrated in Fig. 1(a). Here, mechanical vibrations were produced by the piezoelectric transducer. The procedure for measuring the cutting force is shown in Fig. 1(b). A Kistler dynamometer Type 9257B with a charge amplifier Type 5015 was used to measure the cutting force. The sampling frequency of the recorder was less than the natural frequency of 3.5 kHz which was much less than imposed ultrasonic frequency. The obtained force signals in UAT was effectively averaged over a large number of ultrasonic vibration cycles. The charge amplifier yields proportional voltage data visualised using PicoScope 4424. Force components in three orthogonal directions were measured, namely, in tangential, axial and radial directions, which represent the cutting, feed and thrust forces, respectively (Fig. 1 (a)). An option to machine with minimum quantity lubrication (MQL) was available. Here, a small amount of cutting fluid (UNIST Coolube 2210) was mixed in a flow of compressed air (Fig. 1(c)). Thermal measurement at the cutting zone was obtained from a thermal imaging camera (thermoIMAGER TIM 400) with a resolution of 382 × 288 pixels (Fig. 1(d)). The emissivity of workpiece was calibrated as 0.85 by comparing with a black tape of known emissivity.

In this study, an extruded bar of SiCp/Al MMC was machined, which was essentially an aerospace-grade aluminium (2124Al) reinforced with 25 vol.% SiC particles with a particle diameter, $d \leq 3$ μm distributed in the metal matrix. A representative microstructure of the SiCp/Al composite is shown in Fig. 2. Some of the relevant physical and mechanical properties of the composite are listed in Table 1.

A WC and a PCD cutting tools were selected for the experimental trials; details of the tools are listed in Table 2. From an economic standpoint, PCD inserts are significantly more expensive than WC ones. Thus, cost-effectiveness becomes even more important in machinability of MMCs.

3. Test results and discussions

In this section, machinability aspects such as cutting forces, cutting temperatures, chip formation and surface topography are discussed.

3.1. Machining conditions

To investigate the machinability of SiCp/Al composite, a series of turning experiments were performed in CT and UAT with WC and PCD inserts as listed in Table 3. The effect of coolant (MQL) on machining performance was also studied (tests No. 5 to No. 8 in Table 3). Machining was conducted with a cutting speed (v_c) of 20 m/min, feed rate (f_r) of 0.1 mm/rev and a depth-of-cut (a_p) of 0.1 mm. For machining with ultrasonic assistance, the vibration frequency (f) was 18.11 kHz with a peak-to-peak amplitude (A_{pp}) of 9.3 μm. The critical cutting velocity, above which tool-workpiece separation is lost essentially reducing a UAT process to CT process, was calculated to be 31.7 m/min ($= \pi f A_{pp}$). In our machining trials, easy switching between the CT and UAT regimes was possible, allowing accurate comparisons between the machining processes.

3.2. Cutting forces

The measured signals of cutting forces were processed with an advanced four-channel digital oscilloscope, Picoscope 4424. The data were converted to a format readable in Matlab and filtered to obtain an average cutting force. A typical force response from CT and UAT using a PCD tool is shown in Fig. 3. The force response corresponds to experiments No. 3 and 4 in Table 3. The first 20 s correspond to a time used for tool engagement with the workpiece followed by CT for approximately 40 s, after which ultrasonic vibrations were switched on for another 40 s. Following this, the tool was disengaged. A significant reduction of cutting forces (all three components) was observed when switched to UAT, especially for the main cutting force (tangential direction), which corresponded to ˜58% reduction. A reduction in the thrust and feed forces for UAT was not expected; however, it was observed. This can be explained by the effect of spurious vibrations in the radial and axial directions with low amplitudes (˜1 μm), which are unavoidable in real machining conditions.

Averages of the three force components for each experiment are presented in Fig. 4. Reductions of force components in UAT with different cutting tools and machining conditions (use of lubricants) were obtained. For the WC tool in dry machining conditions, the levels of reduction were 68%, 66% and 25% for cutting, thrust and feed forces, respectively, with ultrasonic assistance when compared to CT. The maximum primary cutting force was observed to decrease from 26.9 N to 8.7 N. When machining with the WC tool and MQL, similar cutting force magnitudes was recorded. With a PCD tool, the net cutting force was lower than that with the WC tool. A possible reason may be due to accelerated rake-face wear of the WC tool in CT, which decreases the effective rake angle leading to the increased cutting force. However, application of UAT resulted in lower tool rake wear and BUE, helping to maintain the original shape of the cutting tool, thus improving cutting performance with both WC and PCD tools. A further discussion about this is in Section 4. When turning with the PCD tool with MQL, the cutting forces in CT were low. Though forces in UAT for such conditions were observed to be lower when compared to those in CT, the reductions were significantly diminished in comparison to all other

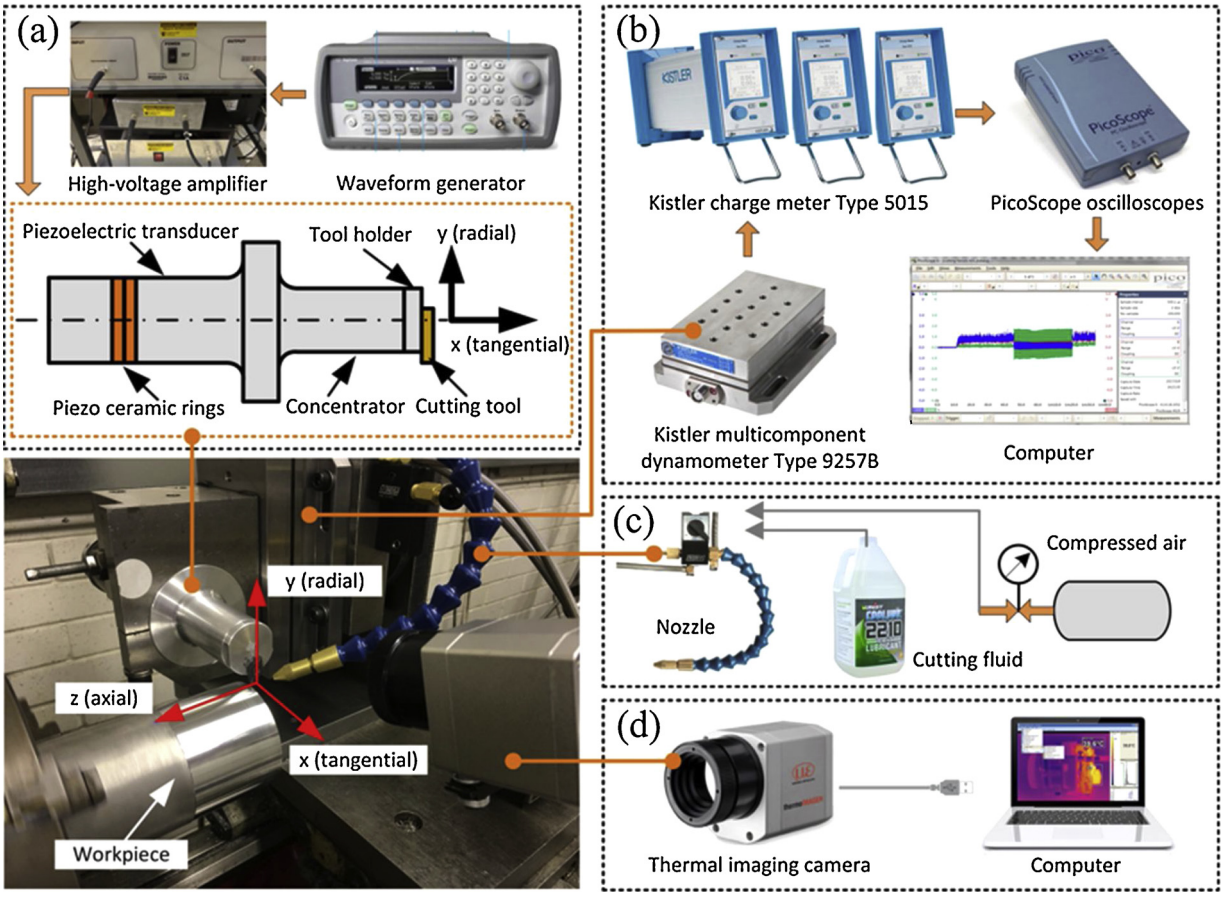

Fig. 1. Experimental setup: (a) ultrasonic-vibration generation system and schematic of ultrasonic machining device; (b) cutting-force measurement system; (c) cooling system; (d) temperature measurement system.

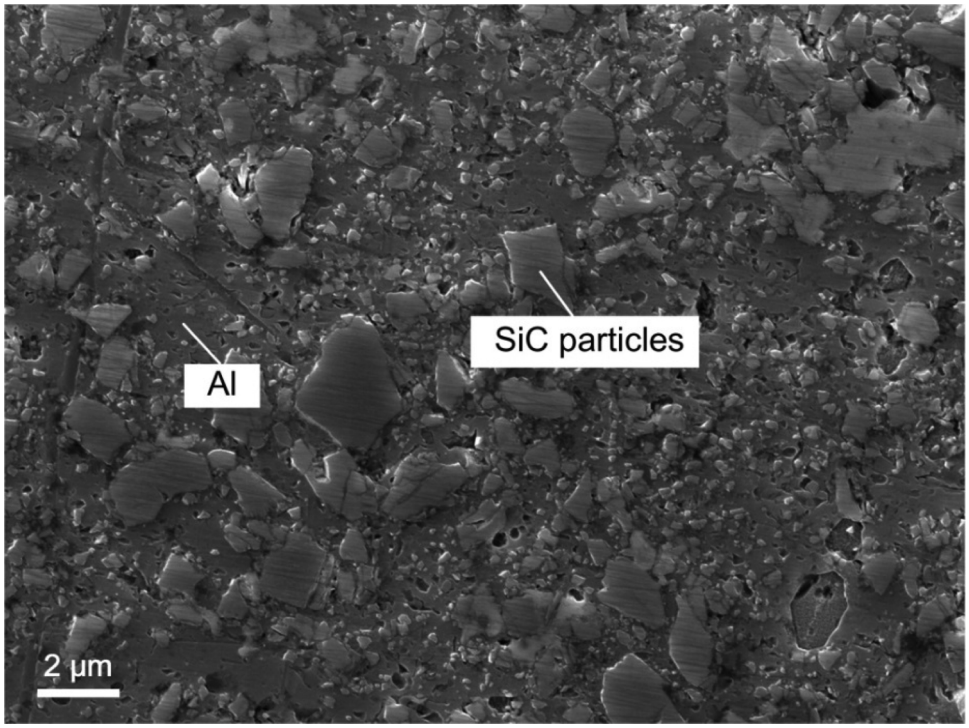

Fig. 2. SEM micrograph of SiCp/Al composite.

Table 1
Properties of SiCp/Al workpiece.

Workpiece Length, mm	126	Workpiece Diameter, mm	71.3
Density, g/cm^3	2.88	Thermal Conductivity, W/ m·°C	150
Elastic Modulus, GPa	115	Thermal Expansion, 10^{-6}/°C	16.1
Specific Stiffness, GPa/(g/cm^3)	39	Solidus, °C	548
Poisson's Ratio	0.3	Specific Heat Capacity, J/g/°C	0.836

Table 2
Cutting-tool specifications.

Toolmaker	SANDVIK	
Tool number	DCMT 11T304-MF1105	DCMW11T304FP CD05
Tool material	WC	PCD
Coating	TiAlN	Uncoated
Nose radius (mm)	0.397	
Rake angle (°)	0	
Clearance angle (°)	7	

Table 3
Machining conditions of turning experiments.

No.	Method	Tool	Machining parameters
1	CT	WC	v_c = 20 m/min
2	UAT		f_r = 0.1 m/rev
3	CT	PCD	a_p = 0.1 mm
4	UAT		f = 18.11 kHz
5	CT + MQL	WC	A_{pp} = 9.3 μm
6	UAT + MQL		
7	CT + MQL	PCD	
8	UAT + MQL		

machining conditions.

3.3. Cutting temperatures

To investigate the temperature in the process zone, a thermal imaging camera was fixed on the feed platform to collect the temperature data for the visible area in real time. Fig. 5 presents the cutting-temperature measurements for CT and UAT with different tools and coolant use. The measurement field resolution was 230 μm/pixel. The white rectangle in each image represents the area where reference temperature (RT) was measured, which was acquired on the surface of the fixture on the feed platform. The maximum temperature (MT) was recorded at the zone indicated by the black rectangle in Fig. 5, which correspond roughly to the tool-tip zone. As seen in Fig. 5, RT at various machining conditions was close to 23 °C. The levels of MT measured during UAT were higher when compared to those in CT for the same cutting tools and coolant use. Muhammad et al. (2014) made a similar observation when machining titanium alloy in CT and UAT. This temperature rise is the result of additional energy transferred by the vibrating tool, which imparts kinetic energy into the process zone, eventually converted into plastic work that leads to an increase in the local temperature. The levels of MT observed in CT (Fig. 5(c)) and UAT (Fig. 5(d)) with a PCD tool were lower than those for the WC tool (Fig. 5(a and b)). There were no significant changes in MT during CT (Fig. 5(e)) and UAT (Fig. 5(f)) with the WC tool and MQL compared to that under dry machining conditions (Fig. 5(a and b)). However, the overall process-zone temperature was lower when machining with MQL. Small reductions of MT in CT (Fig. 5(g)) and UAT (Fig. 5(h)) with PCD tool and MQL were observed compared to those with the same tool under dry machining conditions (Fig. 5(c, d)). This was due to high tool wear in WC (Section 3.6), thus, the use of MQL had some effect on the chip characteristics but negligible effect on cutting force and temperature. In contrast, the coolant had an effect when using PCD tools as they suffer low tool wear. The observations agree well with the trend of cutting forces discussed in Section 3.2.

During the machining tests, an observation was made with regard to CT with the WC tool; light emission, in the form of sparks, occurred with the formation of particle-shaped chips (Fig. 5(a)). In contrast, machining with UAT led to the formation of long unfragmented spring-shaped chips (Fig. 5(b)). A similar observation was made for chips obtained with the PCD tool (Fig. 5(c)) to UAT (Fig. 5(d)). Makhdum et al. (2014) reported that the application of ultrasonic vibration during the machining process enhanced the ductility of the carbon/epoxy composites; a similar effect was observed in machining MMCs. When machining with MQL, no chips are visible in the thermal images (Fig. 5(e–h)) due to their instant removal by a hyperbaric spray.

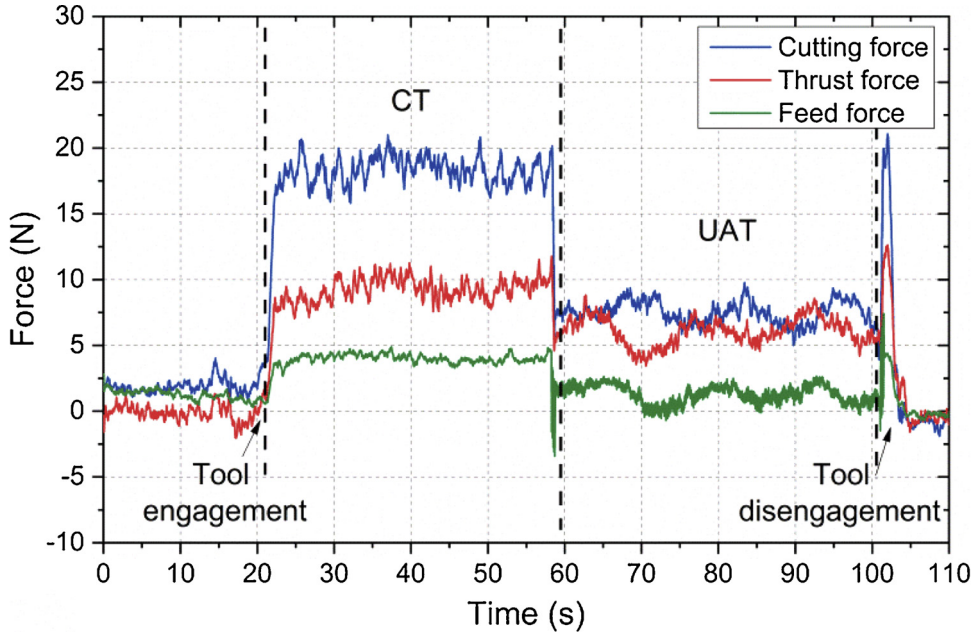

Fig. 3. Typical force evolution in CT and UAT with PCD tool without MQL.

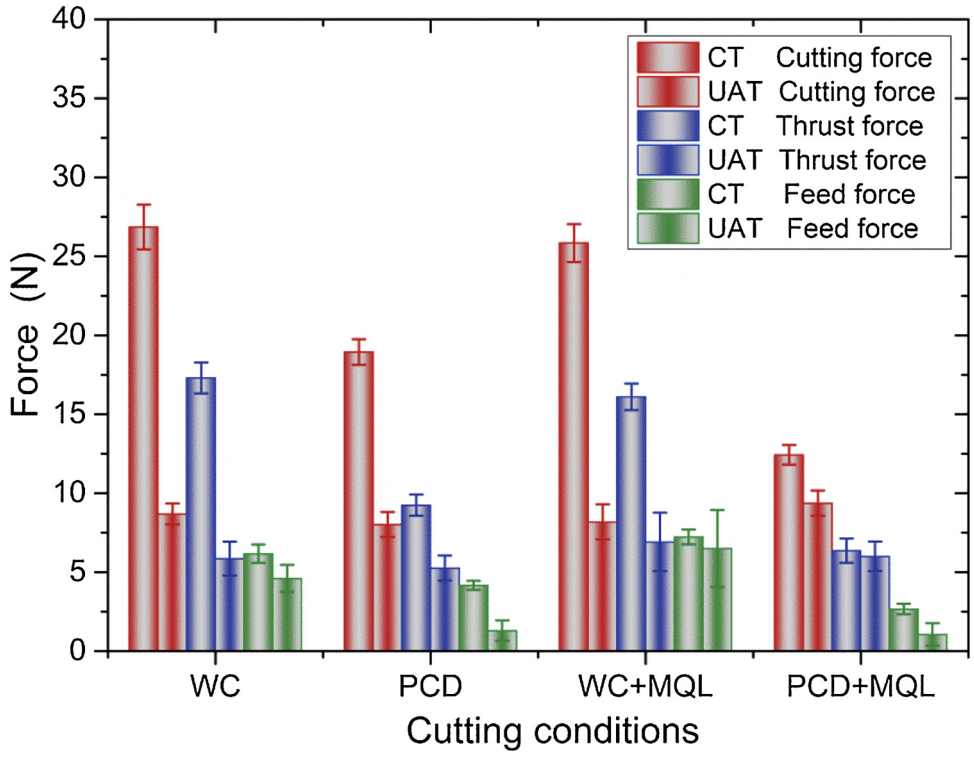

Fig. 4. Cutting forces in CT and UAT with different tools (WC and PCD) and use of lubrication (with and without MQL).

3.4. Chip formation

A study of chip formation and morphology often reveals details of the underlying micro-scale details of the machining process not possible otherwise. Here, the chip morphology obtained from CT and UAT of the MMC with different tools and lubrication is studied (Fig. 6). Chips in the form of particles were generated in CT irrespective of the tool or lubrication condition (Fig. 6(a, c, e, g)). Short C-type chips were formed as observed at the micro level with SEM (Fig. 7(a)). The segmented chips indicate the inherent reduction in ductility of the MMC material caused by the addition of SiC particles. The chip shape was considerably different when ultrasonic vibration was imposed during machining. Long spring-type chips were obtained in UAT with the WC tool (Fig. 6(b)), while semi-continuous chips were formed with the PCD tool (Fig. 6(d)). Short ear-type chips were produced by encountering the as-yet-uncut surface, while long chips of this type were formed by a colliding tool-flank surface. The obtained chips were different from the spring-type chips due to the specific rake-face shape of the WC tool, which encouraged a positive curl. When turning with MQL in UAT, the hyperbaric spray broke off parts of the longer chips, forming shorter ones; thus, the spring-type chip (Fig. 6(b)) changed to the C-type chip (Fig. 6(f)) with the WC tool. When machining with the PCD tool, the mix of long and short ear-type chips (Fig. 6(d)) in dry UAT became short-ear-type-dominated chips with the use of MQL (Fig. 6(h)). Generally, the chips formed in UAT were longer and more continuous than those in CT.

Prior studies discussed the effect of machining conditions on chip formation for metal-matrix composites in CT. Joshi et al. (1999) demonstrated that the increased volume fraction of the hard reinforcement reduced ductility of the MMC when compared to the machining of

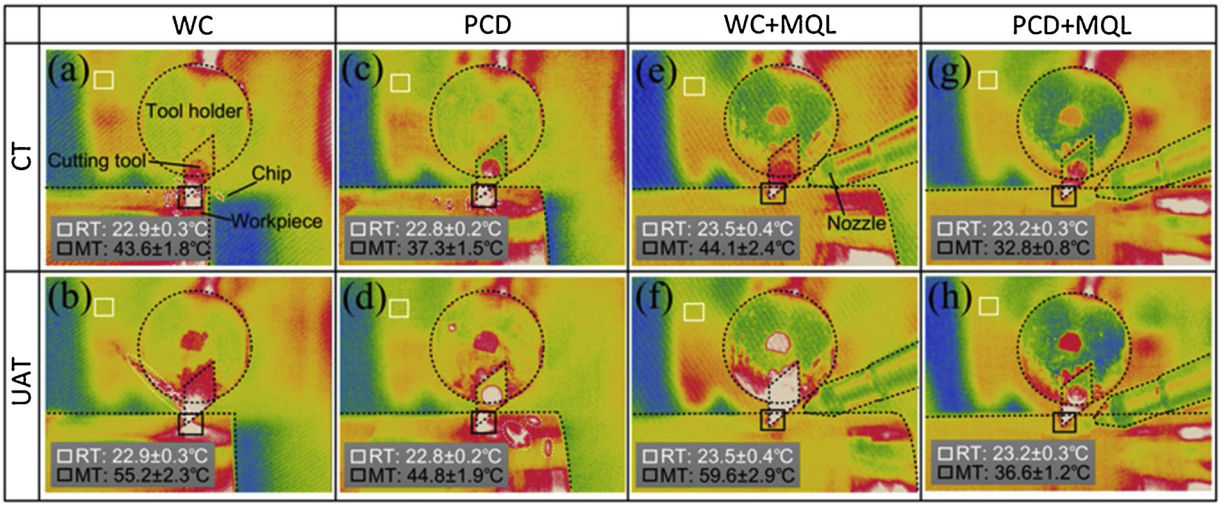

Fig. 5. Cutting temperatures measured with thermal imaging camera in CT and UAT for different cutting regimes and tools.

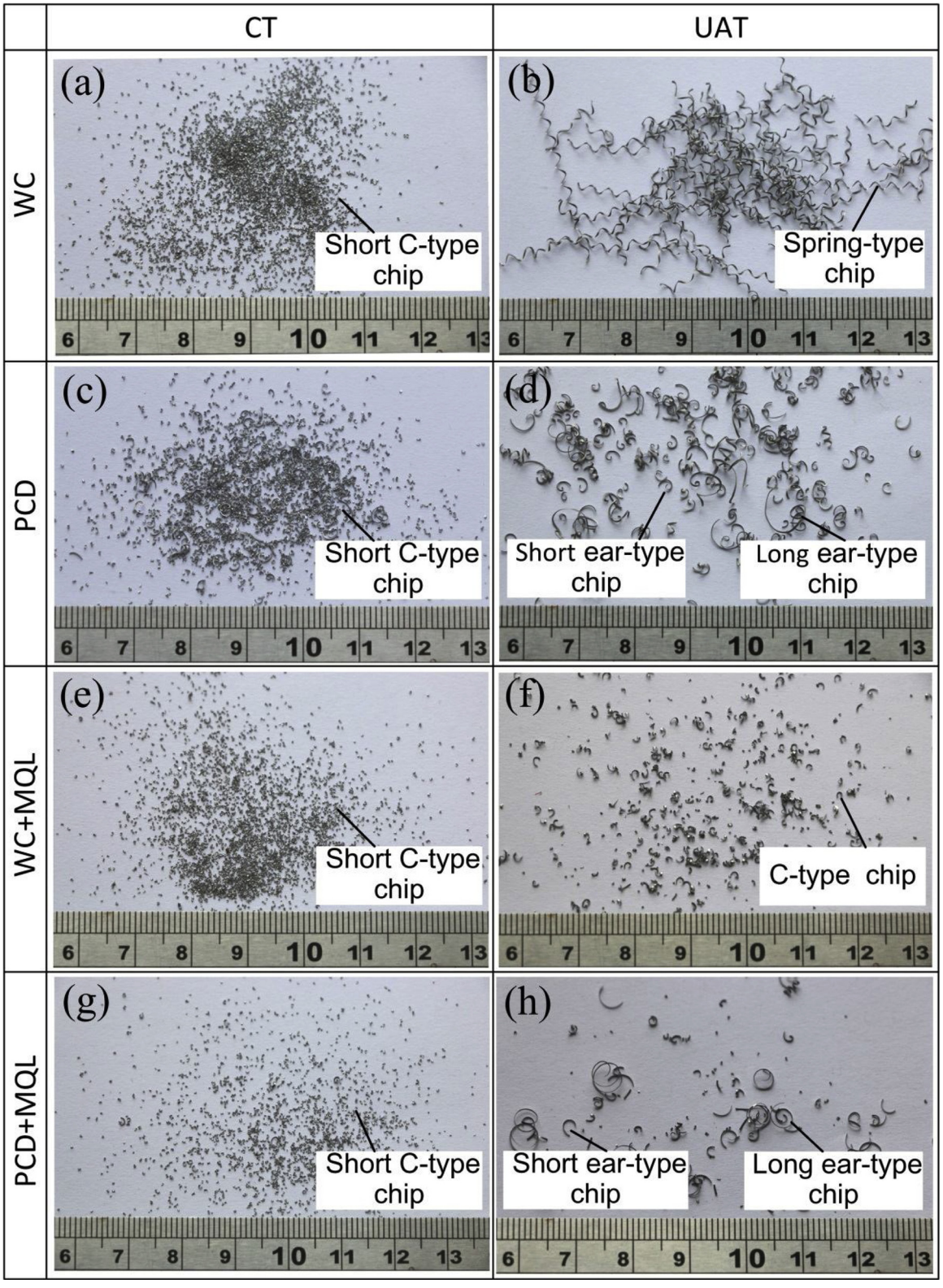

Fig. 6. Chip morphology in CT and UAT with different tools and lubrication conditions.

the matrix metal, favouring chip breakage. Sekhar and Singh (2015) summarized that continuous chips were formed using sharp PCD tools, whereas discontinuous chips were generated with blunt tools or at higher feeds and speeds. The nuances of chip variability with the application of ultrasonic vibration during machining were not studied to date. From our studies, several reasons can be inferred for the observed difference with CT. First, a less prominent BUE and tool abrasive wear were expected in UAT (see Section 4), which maintain the original tool shape, facilitating continuous spring-type chips. Second, a BUE was developed at the tool's rake face in CT, decreasing the effective rake angle, and thus leading to the lower chip curvature, promoting discontinuous chips. Finally, a lower chip-compression ratio was obtained

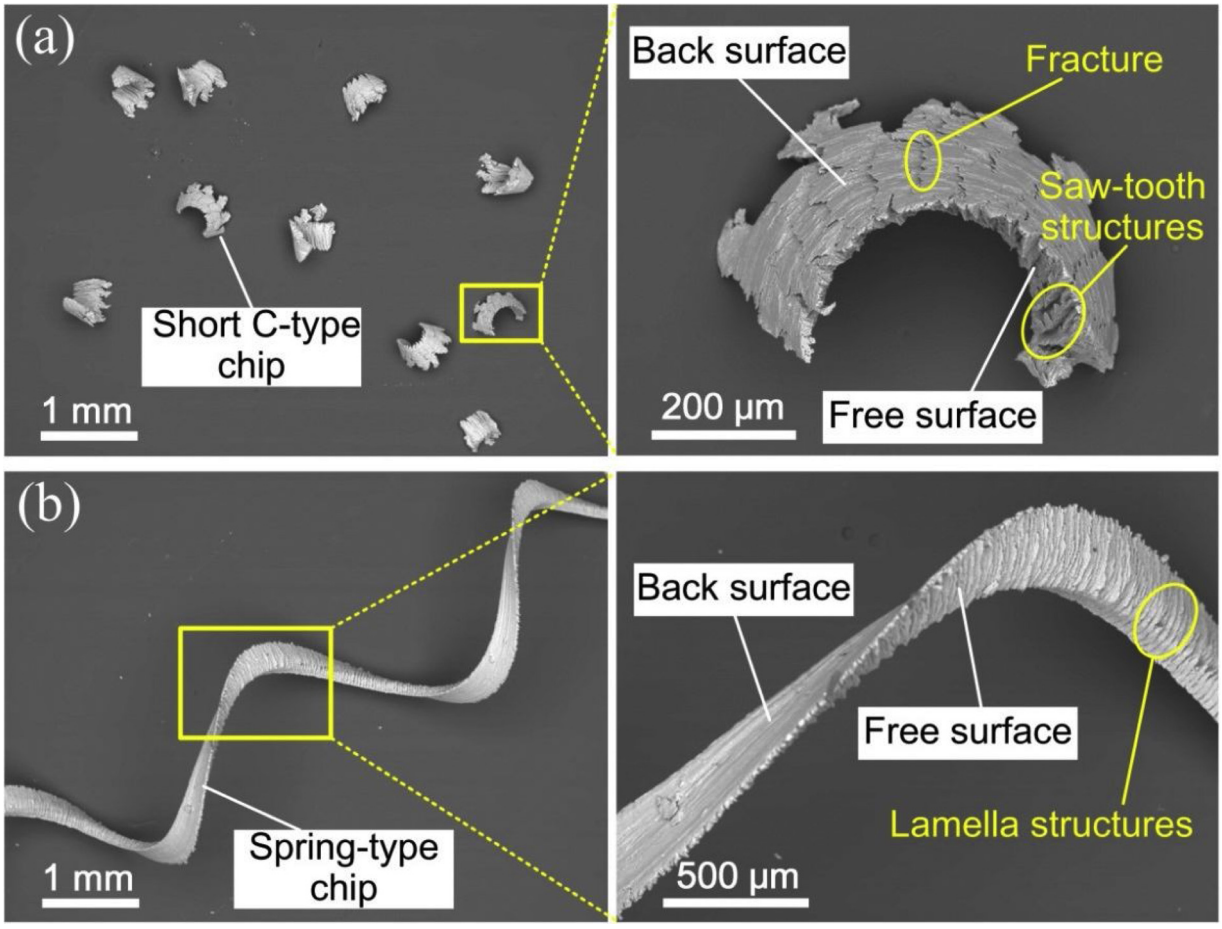

Fig. 7. Chip morphology for WC studied with SEM tool: (a) CT; (b) UAT.

in UAT, implying smaller deformed chip, which corresponds to cutting with a lower feed, favouring continuous chips.

Chip micro-morphology generated by CT and UAT with the WC tool was studied under SEM as shown in Fig. 7. The spring-type chip in UAT (Fig. 7(b)) was significantly different to the short C-type chip in CT (Fig. 7(a)). Chips from CT exhibit saw-tooth features on the free surface, which indicates an adiabatic-shear process dominating chip formation. In UAT, lamella structures appeared on the free surface due to the periodic nature of tool-chip contact, favouring intermittent chip formation. On the back surface of the chip, fractures along the short C-type chip in CT were observed. In contrast, there were no significant flaws on the spring-type chips in UAT. Iuliano et al. (1998) reported that the reinforced particles tend to sink and pile-up in the matrix along the shear planes in the cutting process. Thus, more saw-tooth structures form on the free surface with fractures on the back surface, generating chip segmentation. When turning with ultrasonic vibration, an entirely different mechanism of chip formation was initiated. Bai et al. (2017) also indicated that the microstructure in saw-tooth chip was more uniformly distributed in UAT than in CT. Thus, the reinforced particles in the chip material from UAT were redistributed due to ultrasonic vibrations, thereby preventing their pile-ups along the shear planes, improving the ductility of the chip and resulting in long and continuous chips.

3.5. Surface topography

An optical 3D surface-measurement system (Alicona Infinite Focus G4) was utilized to assess the topography of machined surfaces (Fig. 8). CT with the WC tool showed small-sized craters on the machined surface (Fig. 8(a1, a2)); in contrast, the surface machined with UAT was relatively defect-free (Fig. 8(b1, b2)). This was probably an effect of the change of the effective tool geometry due to generation of BUE in CT, leading to a more abusive machining (hence, the higher cutting forces) when compared to UAT. Hard SiC particles of reinforcement could also contribute to the observed surface fractures. Partially or fully detached from the machined surface, they contributed to the creation of cavities of various sizes and shapes. Some detached particles could move underneath the tool, dragged along the surface for some distance; thus, creating defects larger than their size (~3 μm). As a result of tool vibration in UAT, micro-grooves were formed on the machined surface, corresponding to the vibration amplitude imposed. Machining with the PCD tool showed a lower number of defects on the machined surface obtained with CT (Fig. 8(c1)). A colour surface profile of the machined surface (Fig. 8(c2)) revealed more defects obscured in Fig. 8(c1). Additionally, the machined surface was observed under SEM as shown in Fig. 9. Defects and cracks appeared on the surface machined with the WC tool in CT (Fig. 9(a)). Surprisingly, the machined surface is covered with microcracks when machined with the PCD tool in CT (Fig. 9(b)), although no visible cracks emerged in optical images (Fig. 8(c1)). These micro-defect features were a direct result of the diamond grain size in the PCD tool. The surface machined in UAT with the PCD tool (Fig. 8(d1, d2)) showed fewer undulations when compared to that in CT (Fig. 8(c1, c2)). Compared to dry machining, a slight reduction of defects was obtained on the surface machined in CT with the WC tool with MQL (Fig. 8(e1, e2)). Improvement of surface topography was obtained in UAT (Fig. 8(f1, f2)) in contrast to turning without MQL (Fig. 8(b1, b2)). When turning with the PCD tool with MQL, CT showed a better surface quality (Fig. 8(g1, g2)) than that obtained without lubrication (Fig. 8(c1, c2)). However, no significant changes were observed for UAT with MQL (Fig. 8(h1, h2)) and without it (Fig. 8(d1, d2)).

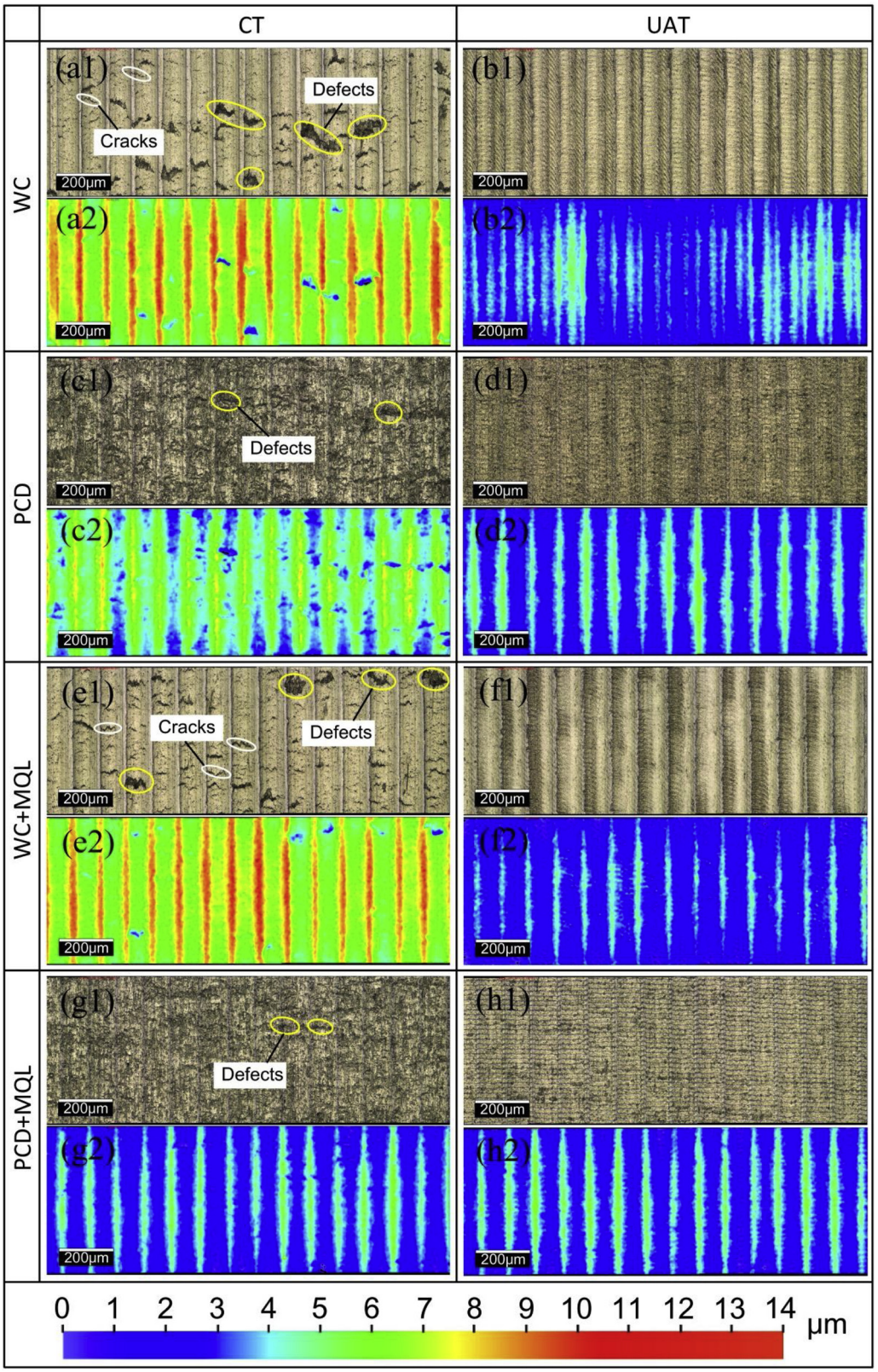

Fig. 8. Comparisons of surface topography with optical (1) and colour (2) patterns for CT and UAT with different tools and lubrication.

Roughness of machined surfaces was also measured and compared for various machining conditions in CT and UAT (Fig. 10). In a CT process, surface roughness obtained with the PCD tool with MQL was the best, followed by the WC tool with MQL, and dry machining with the PCD tool. Surface roughness in case of dry machining with the WC tool was the worst. A significant improvement in R_a of 44.3% was obtained in UAT with the WC tool (when compared to CT with the same machining conditions) and 31.8% with the WC tool and MQL. The results obtained for the PCD tool are somewhat different. In UAT, a 13.6% improvement in R_a was observed for the dry machining conditions.

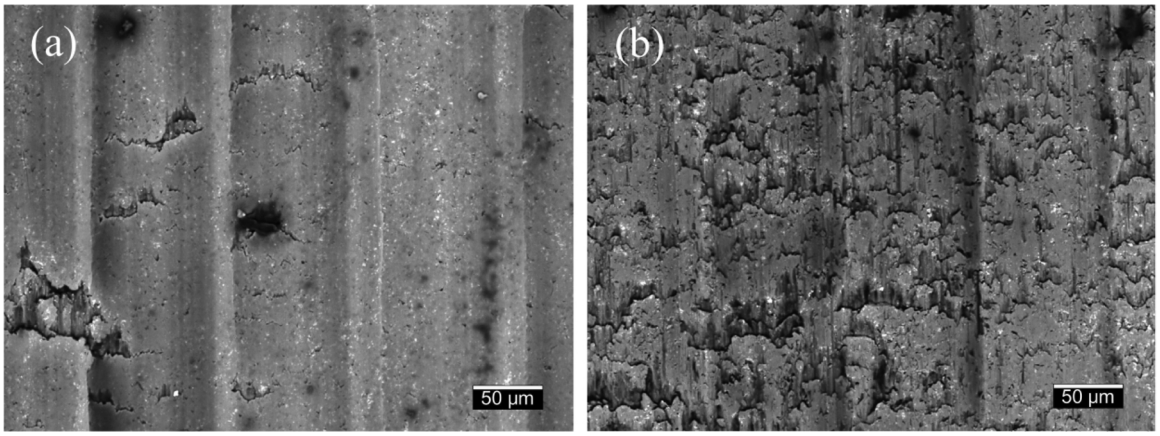

Fig. 9. Microstructure of machined surface in CT with WC (a) and PCD (b) tools.

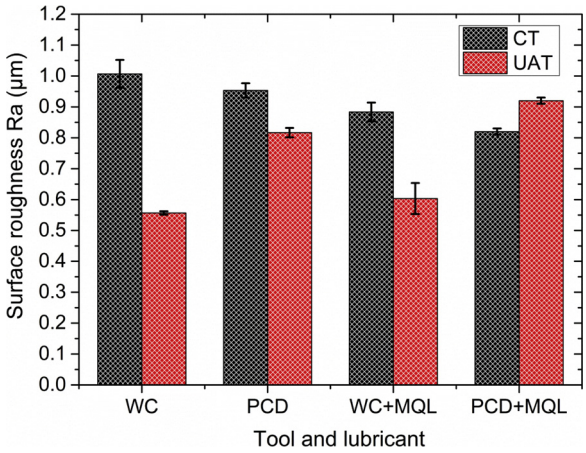

Fig. 10. Comparisons of surface roughness for various machining conditions in CT and UAT.

However, with the MQL use, the surface roughness deteriorates in UAT, showing a 12.2% increase in R_a when compared to surface topography obtained in CT. Comparing the nominal surface roughness obtained for all machining conditions, it was observed that the surface quality using the WC tool and with ultrasonic assistance far outperformed the quality obtained with the PCD tool with MQL application using conventional machining. This observation is encouraging, especially from the aspect of machining economics as the WC tool is significantly cheaper than a PCD tool. Additionally, dry machining is preferred as it contributes directly to sustainable manufacturing.

3.6. Tool wear

To examine the tool performance for the varying machining conditions studied, tool geometry was observed before and after machining using SEM (Fig. 11). Tool geometries of as-received WC and PCD tools are shown in Fig. 11(a and b), respectively. The tool inserts both had a rake angle of 0°, a clearance angle of 7° and a nose radius of ˜0.4 mm (Table 2). It should be mentioned that a new cutting tool was used in each turning test with four different process conditions. However, these cutting tools were not replaced when the process was switched from CT to UAT in each run. A total processing time before wear measurement was less than 100 s. This means that Fig. 11(b, c, e and f) present the tool wear after machining with both CT and UAT for various process conditions. In turning with the WC tool, wear occurred on both rake and flank surfaces, with and without lubrication (Fig. 11(b and c)). A BUE was generated on the rake face and the tool edge in dry turning with this tool (Fig. 11(b)), while lubricating with MQL, resulted in a smaller BUE and a worn area (Fig. 11(c)). In contrast, tool wear was limited when turning with the PCD tool (Fig. 11(e and f)), since it is a significantly harder material than WC. However, though less in volume, BUE was observed to form on the PCD tool with MQL (Fig. 11(f)).

Clearly, the presented machining methodology was not fully suitable for revealing differences in the rate and mechanisms of wear in CT and UAT. Therefore, a thorough tool wear analysis was performed additionally to study the specific nature of tool wear in both turning techniques with and without lubrication.

4. Wear analysis

To study different tool-wear mechanisms in CT and UAT with the WC and PCD tools, a set of experiments was performed. Table 4 lists the detailed machining conditions of these experiments. Experiments No. 9 and No. 10 were performed without any coolants (dry conditions) with the WC tool in CT and UAT, respectively. Prior experiments (Section 3) show that the best conventional machining was obtained with a PCD tool and with MQL use. Therefore, experiment No. 11 was set as a benchmark for comparison.

To study the wear evolution of cutting tools, the tool geometry was observed using SEM at various stages of machining. First, wear was assessed at an axial cutting length of 20 mm, corresponding to a cutting distance of ˜42 m. Finally, it was studied after the tool was completely worn. In addition, roughness on the machined surface was measured after every 10 mm of axial cutting length after continuous turning.

The initial state of wear of the WC tool subjected to CT and UAT are shown in Fig. 12(a and b), respectively. Worn areas of comparable sizes emerged on both the rake and flank faces of the tools. However, BUE formation was larger in CT than that in UAT. No noticeable wear was observed on the PCD tool with lubrication in CT, as shown in Fig. 12(c). Therefore, from the perspective of integrity of tool geometry, the PCD tool combined with MQL presented the best abrasion resistance, followed by the WC tool in UAT and in CT. Interestingly, the machined surfaces of SiCp/Al show that the level of surface roughness (R_a) obtained in UAT using the WC tool was 0.65 μm, much less than that obtained in CT with the WC tool and the PCD tool with MQL. Therefore, even with a higher tool wear, UAT with the WC yielded better surface topography.

To further assess the wear mechanism of the WC tool in turning with and without ultrasonic assistance, the EDS spectrum of tool tip was determined (Fig. 13). Spectrum 1 shows the elemental constituents at the spatial point on the tool flank surface (Figs. 13(a and b)). The presence of N, Al and Ti in Spectrum 1 for both CT and UAT indicate that this area was covered by the specific tool coating used (TiAlN). The weight fraction of C is 42.2% in CT-in comparison to 9.1% in UAT-shows that due to the increased wear in CT, the underlying WC matrix

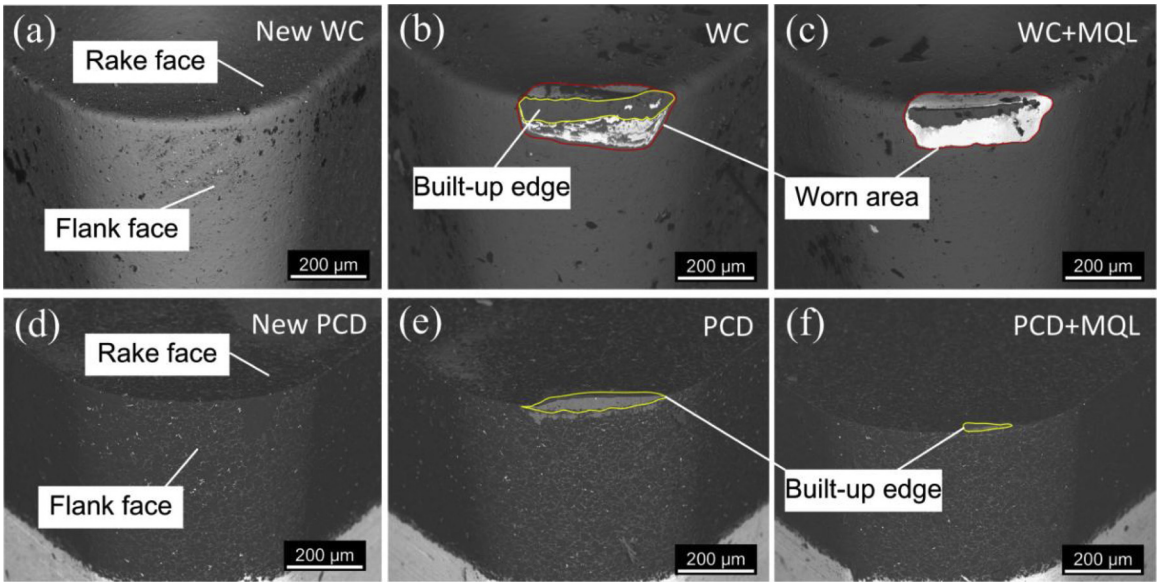

Fig. 11. SEM images of tool wear: (a) WC tool before machining; (b) WC tool after dry turning; (c) WC tool after turning with MQL; (d) PCD tool before machining; (b) PCD tool after dry turning; (c) PCD tool after turning with MQL.

Table 4
Machining conditions of turning experiments for tool wear.

No.	Method	Tool	Coolant	Machining parameters
9	CT	WC	Dry	v_c = 20 m/min
10	UAT	WC	Dry	f_r = 0.1 m/rev
11	CT	PCD	MQL	a_p = 0.1 mm
				f = 18.19 kHz
				A_{pp} = 8 μm

material was exposed. Spectrum 2 was chosen on the worn part of tools. The major elemental concentration was for W and C, indicating that the tool coating (TiAlN) was completely removed, with the tool matrix (WC) present in both tool tips. 15.7% of Al in this area for CT was due to adherence of the workpiece material. Thus, the major wear mechanism was abrasive wear for both tools. Spectrum 3 shows the element concentration at the BUE. The top three elements in terms of weight fraction were Al, C and Si; therefore, it can be concluded that the BUE was formed by SiCp/Al workpiece material, indicating adhesion wear. Other species such as O were from an oxide layer and Co from the binder material. Thus, both abrasive and adhesion wear occurred in the WC tools in CT and UAT.

At an axial cutting length of 200 mm, the WC tool was considered to be completely worn as the cutting-force signal became very large during CT. Tool wear for other machining conditions was also assessed at this cutting length. The states of tool wear of the three cutting tools were observed with SEM (Fig. 14). In comparison to the initial wear stage (Fig. 12), the tool wear showed significant changes. The WC tool in CT (Fig. 14(a)) was totally worn, with a significant volume of the cutting tool tip missing. In contrast, the WC tool used in UAT was more worn out (Fig. 14(b)) than at the initial stage (Fig. 12(b)), yet it was less than that in CT. Also, less BUE appeared on the WC tool in UAT than in CT. Some BUE was observed on the rake face of the PCD tool with no observable abrasive wear (Fig. 14(c)). Roughness of the machined surface by the three processes is presented in Fig. 14(d). The surface roughness was worse in CT, while the other two processes achieve almost similar surface topography.

Progressive surface roughness (R_a) of the machined surface was measured for every 10 mm in the axial direction; the respective machined length can be calculated based on the effective cutting speed. The variation of the surface roughness with the actual cutting length is presented in Fig. 15 for the three machining conditions. The obtained results indicate no obvious trend, with surface roughness fluctuating along the cutting length. This in part was due to varying wear stages of the cutting tools: the removal of the coating was followed by abrasive wear and BUE effect that often occur in rapid succession.

In summary, the WC tool in UAT demonstrated an overall superior performance when compared to the CT processes. Compared to the outcome of conventional machining with the PCD tool with MQL, the performance of the WC tool in dry UAT was noteworthy. Though the tool suffered higher wear, the machining-induced surface roughness was comparable-and sometimes even better-than in case of the PCD tool. Thus, the use of significantly cheaper WC tools with the UAT technique may be a viable way for economic and sustainable machining of SiCp/Al composites.

5. Conclusions

In this study, the machinability of SiC-particle-reinforced aluminium-matrix composite with WC and PCD tools in ultrasonically assisted turning was investigated. Based on the results obtained, the following conclusions may be drawn:

1) UAT achieved a significant reduction of cutting forces, with a slight increase of cutting temperature. Continuous and semi-continuous chips with better surface topography were obtained. The exception to this observation was the case with the use of the PCD tool and MQL. Under such a machining condition, CT was better.
2) The use of MQL showed no observable improvement of cutting forces, surface roughness and topography of the machined surface. It was effective in lowering the cutting-zone temperature moderately, changing the chip morphology and reducing the generation of the BUE.
3) The chip-formation mechanism in UAT confirmed increased ductility of the workpiece material when subjected to a repeated high frequency microchipping process. The chips obtained in UAT were continuous and semi-continuous in nature.
4) Comparisons of the machined surface for CT and UAT demonstrated defects appearing in CT, whereas in UAT the machined surface was of higher quality.
5) Abrasive and adhesive wears occurred on the WC tool in both CT and UAT. However, the machined surface obtained in UAT with the

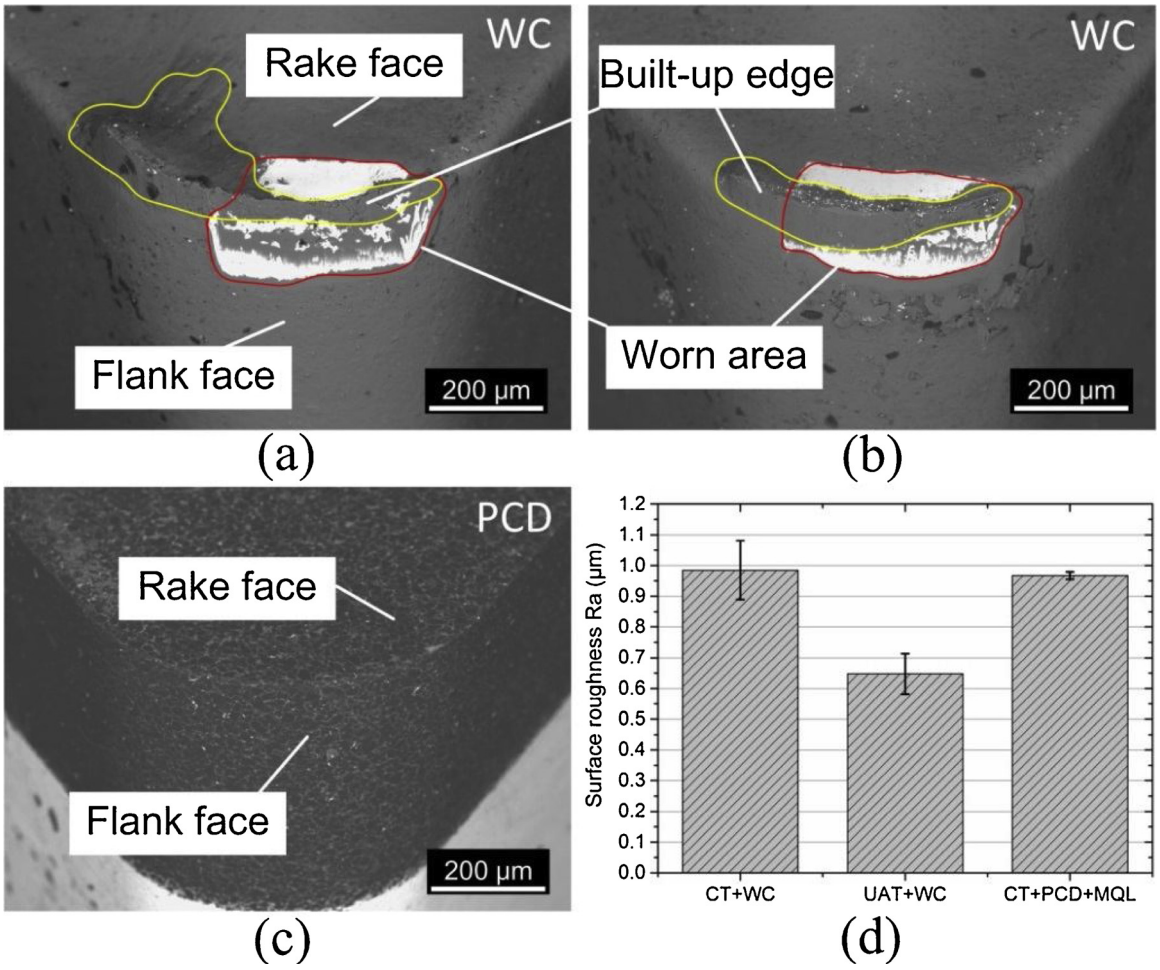

Fig. 12. Initial wear state of cutting tools after machining axial distance of 20 mm: (a) CT with WC tool; (b) UAT with WC tool; (c) CT with PCD tool and MQL. (d) Surface roughness of machined surface.

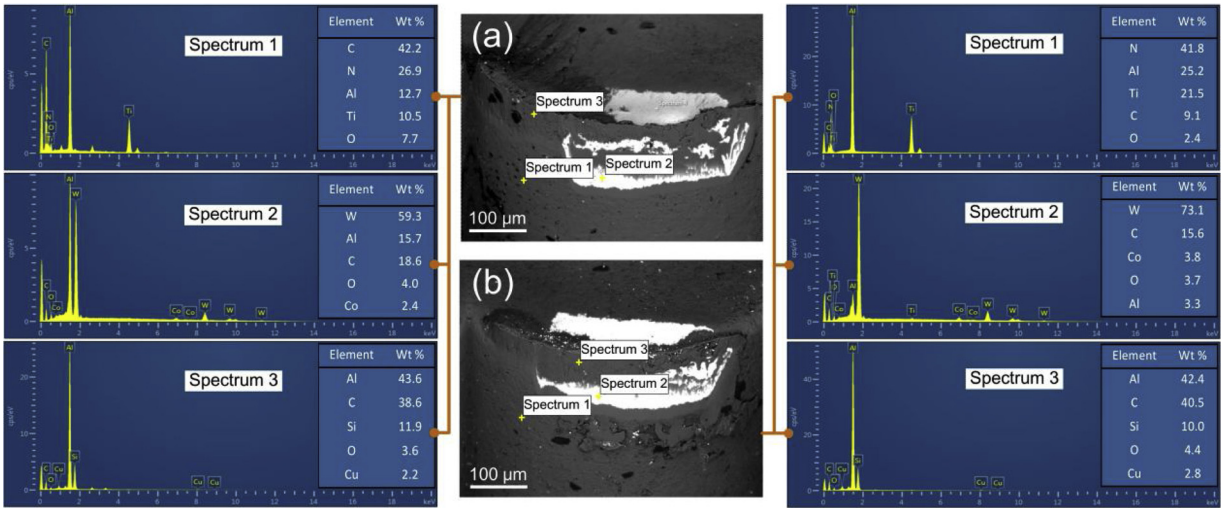

Fig. 13. EDS spectrum of WC tool tip: (a) CT; (b) UAT.

WC tool was comparable and sometimes even better than that achieved with the PCD tool.

Our studies show that UAT is a viable and efficient machining process for turning MMCs such as SiC-reinforced Al-composites. In the future, we plan to study the nature of residual stresses in the MMC induced by the machining processes. Studies with different imposed ultrasonic frequency and amplitude can also be performed. In the present study, the chosen frequency and amplitude was optimised based on the specific ultrasonic transducer used.

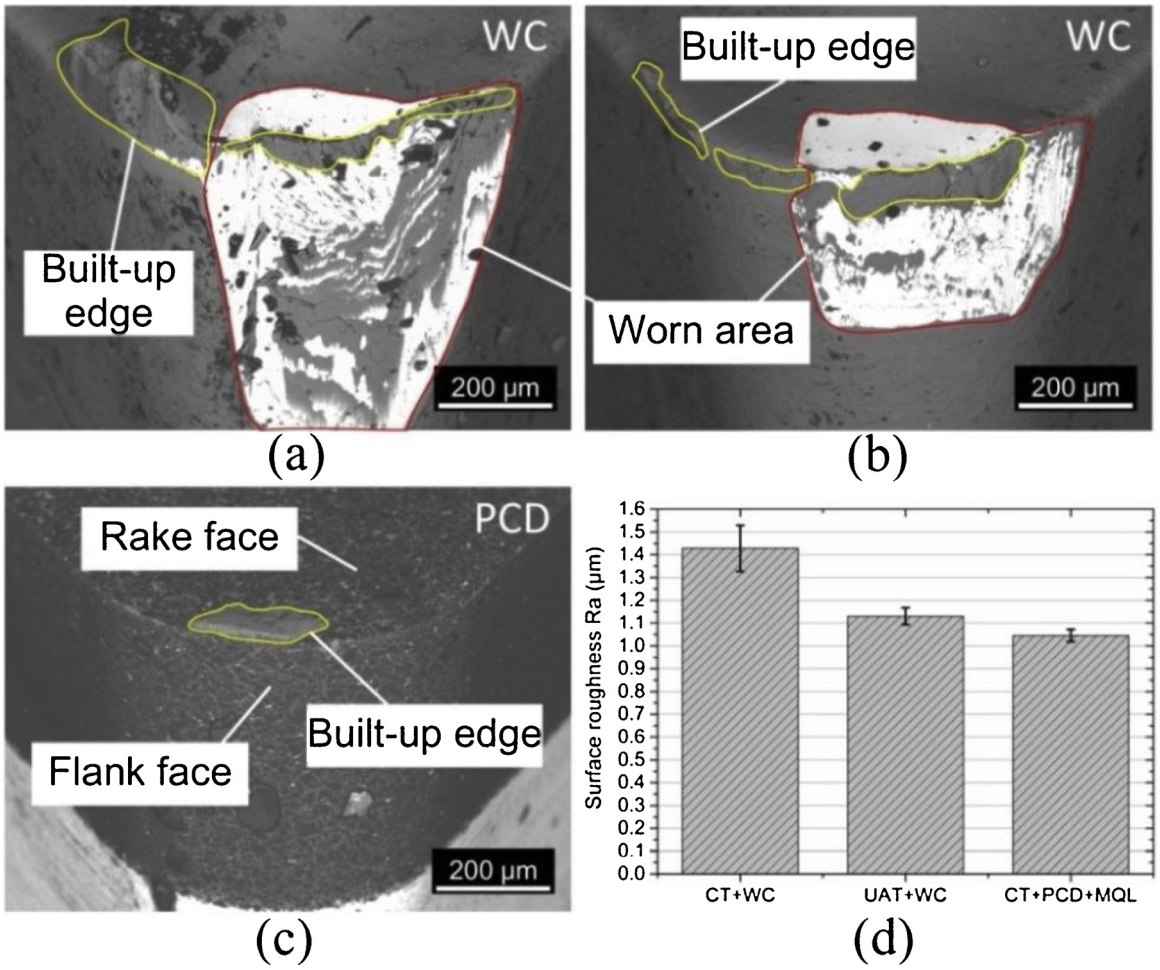

Fig. 14. Final wear stage of cutting tools: (a) CT with WC tool; (b) UAT with WC tool; (c) CT with PCD tool and MQL. (d) Final surface roughness of machined surface.

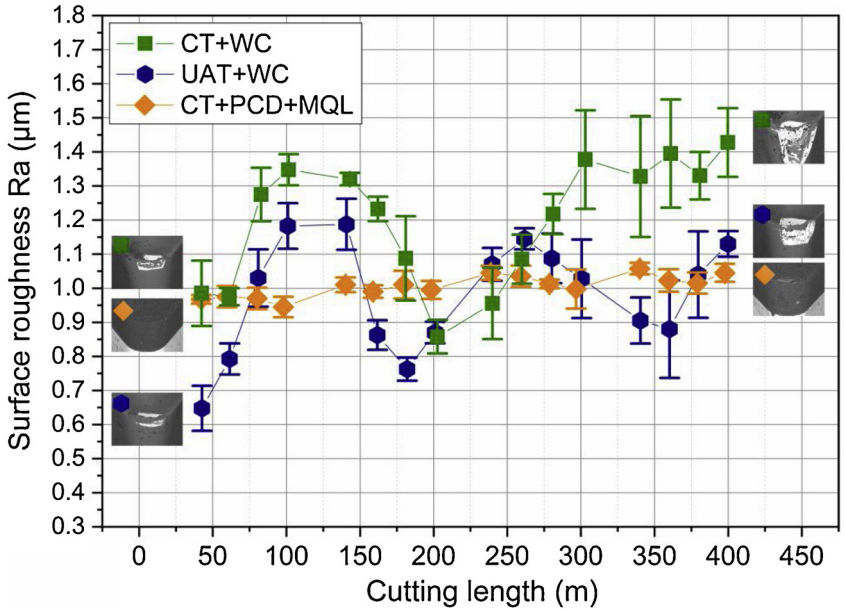

Fig. 15. Surface roughness versus cutting length for three machining conditions.

Acknowledgements

This work was supported by the National Basic Research Program of China (973 Program) grant No. 2013CB035805. The authors gratefully acknowledge financial support by the China Scholarship Council. Funding from the Engineering and Physical Sciences Research Council (UK) through grant EP/P027555/1 is gratefully acknowledged. Assistance of Mr Panayiotis Antoniou with some of the experimental

studies is gratefully acknowledged.

References

Babitsky, V.I., Kalashnikov, A.N., Meadows, A., Wijesundara, A., 2003. Ultrasonically assisted turning of aviation materials. J. Mater. Process. Technol. 132, 157–167.
Bai, W., Sun, R., Leopold, J., Silberschmidt, V.V., 2017. Microstructural evolution of Ti6Al4V in ultrasonically assisted cutting: numerical modelling and experimental analysis. Ultrasonics 78, 70–82.
Basavarajappa, S., Chandramohan, G., Rao, K.N., Radhakrishanan, R., Krishnaraj, V., 2006. Turning of particulate metal matrix composites—review and discussion. Proc. I. Mech. Eng. B-J. Eng. 220, 1189–1204.
Bhushan, R.K., Kumar, S., Das, S., 2010. Effect of machining parameters on surface roughness and tool wear for 7075 Al alloy SiC composite. Int. J. Adv. Manuf. Technol. 50, 459–469.
Chawla, N., Shen, Y.-L., 2001. Mechanical behavior of particle reinforced metal matrix composites. Adv. Eng. Mater. 3, 357–370.
Dabade, U.A., Joshi, S.S., 2009. Analysis of chip formation mechanism in machining of Al/SiCp metal matrix composites. J. Mater. Process. Technol. 209, 4704–4710.
El-Gallab, M., Sklad, M., 1998. Machining of Al/SiC particulate metal matrix composites: Part II: workpiece surface integrity. J. Mater. Process. Technol. 83, 277–285.
Hocheng, H., 2011. Machining Technology for Composite Materials: Principles and Practice. Elsevier.
Iuliano, L., Settineri, L., Gatto, A., 1998. High-speed turning experiments on metal matrix composites. Compos. Part A 29, 1501–1509.
Joshi, S., Ramakrishnan, N., Ramakrishnan, P., 1999. Analysis of chip breaking during orthogonal machining of Al/SiCp composites. J. Mater. Process. Technol. 88, 90–96.
Lin, C., Hung, Y., Liu, W.-C., Kang, S.-W., 2001. Machining and fluidity of 356Al/SiC (p) composites. J. Mater. Process. Technol. 110, 152–159.
Makhdum, F., Phadnis, V.A., Roy, A., Silberschmidt, V.V., 2014. Effect of ultrasonically-assisted drilling on carbon-fibre-reinforced plastics. J. Sound Vib. 333, 5939–5952.
Manna, A., Bhattacharayya, B., 2003. A study on machinability of Al/SiC-MMC. J. Mater. Process. Technol. 140, 711–716.
Maurotto, A., Muhammad, R., Roy, A., Silberschmidt, V.V., 2013. Enhanced ultrasonically assisted turning of a β-titanium alloy. Ultrasonics 53, 1242–1250.
Muhammad, R., Hussain, M.S., Maurotto, A., Siemers, C., Roy, A., Silberschmidt, V.V., 2014. Analysis of a free machining α + β titanium alloy using conventional and ultrasonically assisted turning. J. Mater. Process. Technol. 214, 906–915.
Ozben, T., Kilickap, E., Cakır, O., 2008. Investigation of mechanical and machinability properties of SiC particle reinforced Al-MMC. J. Mater. Process. Technol. 198, 220–225.
Sekhar, R., Singh, T., 2015. Mechanisms in turning of metal matrix composites: a review. J. Mater. Res. Technol. 4, 197–207.
Zhao, B., Liu, C.S., Zhu, X.S., Xu, K.W., 2002. Research on the vibration cutting performance of particle reinforced metallic matrix composites SiCp/Al. J. Mater. Process. Technol. 129, 380–384.
Zhong, Z.W., Lin, G., 2006. Ultrasonic assisted turning of an aluminium-based metal matrix composite reinforced with SiC particles. Int. J. Adv. Manuf. Technol. 27, 1077–1081.